International Journal of Remote Sensing

ISSN: 0143-1161 (Print) 1366-5901 (Online) Journal homepage: http://www.tandfonline.com/loi/tres20

Spatiotemporal pattern analysis of potential light seine fishing areas in the East China sea using VIIRS day/night band imagery

Lingwei Luo, Mengjun Kang, Jinhui Guo, Ying Zhuang, Zebin Liu, Yameng Wang & Liping Zou

To cite this article: Lingwei Luo, Mengjun Kang, Jinhui Guo, Ying Zhuang, Zebin Liu, Yameng Wang & Liping Zou (2018): Spatiotemporal pattern analysis of potential light seine fishing areas in the East China sea using VIIRS day/night band imagery, International Journal of Remote Sensing

To link to this article: https://doi.org/10.1080/01431161.2018.1524605

Published online: 22 Oct 2018.

INTERNATIONAL JOURNAL OF REMOTE SENSING
https://doi.org/10.1080/01431161.2018.1524605

Spatiotemporal pattern analysis of potential light seine fishing areas in the East China sea using VIIRS day/night band imagery

Lingwei Luo[a,b], Mengjun Kang[a], Jinhui Guo[c,d], Ying Zhuang[a], Zebin Liu[a], Yameng Wang[c] and Liping Zou[e]

[a]School of Resource and Environmental Sciences, Wuhan University, Wuhan, China; [b]Laboratory for Earth Surface Processes, Ministry of Education, College of Urban and Environmental Sciences, Peking University, Beijing, China; [c]School of Remote Sensing and Information Engineering, Wuhan University, Wuhan, China; [d]Institute of Remote Sensing and GIS, Peking University, Beijing, China; [e]Data Production Center, Leador Spatial Information Technology Corporation, Wuhan, China

ABSTRACT

Light seine fishing, one of the most efficient methods used in modern fisheries, is performed based on fish phototaxis. In this study, the East China Sea was selected as the study area, and fishing vessel pixels (pixels representing light seine fishing vessels) were detected in five years of Visible Infrared Imaging Radiometer Suite (VIIRS) day/night band (DNB) imagery according to three indicators: the Spike Median Index (SMI), Sharpness Index (SI), and Spike Height Index (SHI). Subsequently, cluster, barycenter, range and direction, and density analyses were conducted to comprehensively evaluate the spatiotemporal patterns of potential light seine fishing areas in the East China Sea. The following conclusions were drawn from the study: (1) the number of fishing vessel pixels exhibited obvious monthly characteristics that are consistent with the fishing moratorium that has been enforced in this region; (2) at the study area scale, light seine fishing occurred in one cluster, and the pattern in the interior of the cluster exhibited spatiotemporal periodicity; (3) the barycenter of the fishing areas displayed opposing movement trends in the first half and the second half of the year, and the movements were closely linked to water temperature changes. In addition, seasonally concentrated fishing areas were observed in winter, spring and summer; (4) the peak fishing month advanced from September to August beginning in 2014, and the fishing areas displayed a strong tendency in orientation that was highly consistent with the distribution of the Kuroshio Front in the East China Sea; and (5) light seine fishing activities were mainly concentrated in the second half of the year, especially in summer, but the intensity has declined in recent years. Our results are in good agreement with the results of other scholars and provide reliable information concerning where and when light seine fishing occurs. These results also suggest that VIIRS DNB imagery can be effectively used to detect light seine fishing areas.

ARTICLE HISTORY
Received 29 March 2018
Accepted 3 September 2018

CONTACT Mengjun Kang mengjunk@whu.edu.cn School of Resource and Environmental Sciences, Wuhan University, Wuhan, China

1. Introduction

Light seine fishing, which is one of the most efficient fishing methods in modern fisheries, utilizes high-intensity lighting to capture fish based on their phototaxis (Chen et al. 2013). Because of the wide range of light seine fishing methods, dozens of tons of fish can be caught at one time, making the method extremely efficient. Light seine fishing vessel fleets usually include the main light boat, with a total power that can reach hundreds of kilowatts, and many secondary light boats, with a total power that can reach 1 kW. When fishing, the high-power lights are arranged on the surface and underwater to attract the fish. When numerous fish gather around the lights, the fishermen cover the fish with a large net. In the world's oceans, the high-powered light emitted by fishing boats is visible in nighttime light imagery (Rodhouse, Elvidge, and Trathan 2001) and is the main source of marine luminosity (Li and Li 2015). Japan, the United States, Russia, Norway, Australia, and Peru are all technologically advanced in terms of light seine fishing. However, with the development of fishery technologies, including light seine fishing, some areas are gradually suffering from overfishing. For example, the catch abundance in the East China Sea has obviously declined in recent years, and there have been reports that the East China Sea is facing a 'fish shortage'. These observations indicate that fishery resources are suffering from excessive fishing (Wang, Zheng, and Cungen 2014). To maintain the sustainability of fishery resources in the East China Sea, efficient and effective management must be implemented, and detecting fishing areas could be a good management method.

Spatial patterns are important attributes of fishing areas that can be used to study the structure of fish populations and the relationships among fish populations (Berkeley et al. 2004). Currently, fishery research methods mainly involve habitat environment research and spatiotemporal analysis (Gauthierouellet et al. 2009; Leeney et al. 2008; Marttila, Kyllönen, and Karjalainen 2016; Van, Griffioen, and van Keeken 2017). Habitat environment research involves measuring abiotic environmental factors that affect fish behaviour, including the sea surface temperature (SST), chlorophyll (Chl-a) concentration, sea surface salinity, water depth, and seabed conditions (Cole and Villacastin 2000; Maravelias, Reid, and Swartzman 2000; Paulino, Segura, and German 2016; Solanki, Bhatpuria, and Chauhan 2015; Wang et al. 2010). Because the habitats and environments of marine fish are typically unified, changes in the habitat environmental index have an obvious influence on fish in terms of their size, distribution, and habitat level, as well as on fishery hotspots (Yu et al. 2016; Yasuda, Ohshimo, and Yukami 2014). The Habitat Suitability Index (HSI) model has been used to simulate the response of organisms to their surrounding habitat and in species management and fish distribution analyses (Vinagre et al. 2006; Li et al. 2016). In addition, it has been used to analyse fisheries (Chang et al. 2012; Chen et al. 2009), with satisfactory results. In this model, SSTs and Chl-a concentrations represent important environmental factors that allow scholars to determine fishery changes and predict the locations of fishery hotspots (Kumari and Raman 2010; Li et al. 2014; Yen et al. 2012; Silva et al. 2016). However, a common drawback of the above studies is the use of a limited number of environmental factors. In the complicated conditions of the East China Sea, accurate predictions and simulations remain difficult. Furthermore, the previously published studies required fishing data that were not easy to obtain, and the detection and analysis of such data are not timely, rapid or dynamic.

In recent years, the National Centers for Environmental Information (NCEI) (formerly the National Geophysical Data Center) have begun to provide digital image data for the Defense Meteorological Satellite Program's operational linescan system (DMSP-OLS), and some scholars have begun to conduct spatiotemporal research on fishery resources using the DMSP-OLS imagery (Kiyofuji et al. 2001; Choi et al. 2008). Furthermore, many researchers have utilized nighttime light data to determine the quantity and movement of light seine fishing vessels (Cho et al. 1999; Kiyofuji and Saitoh 2004; Waluda, Griffiths, and Rodhouse 2008). Waluda et al. (Waluda et al. 2004) concluded that the distribution of the fishing vessel fleet derived from nighttime light imagery closely resembled that derived from ship location data, demonstrating the feasibility of using nighttime light imagery to study fishery movements. Compared with habitat environment factors, nighttime light images more directly reflect changes in the fishery, and similar approaches can be easily extended to other areas because of their global scope (Rodhouse, Elvidge, and Trathan 2001).

However, DMSP-OLS imagery is of low spatial resolution and often lacks sensor radiation calibration. These defects have limited the accuracy of predicting and simulating fisheries. This problem has been alleviated with the launch of a new satellite in 2011 as part of the Suomi National Polar-orbiting Partnership. This satellite was equipped with the first Visible Infrared Imaging Radiometer Suite (VIIRS). The VIIRS day/night band (DNB) receives information and can be used to optimize the low-light detection capability of DMSP-OLS. Compared with DMSP-OLS data, VIIRS DNB data have a smaller instantaneous field of view, more greyscale pixels and a higher spatial resolution. Furthermore, the radiation corrections applied to the DNB are consistent with those of the other VIIRS bands. Recent works have shown that the ability of the VIIRS sensor to detect lights from fishing vessels is satisfactory. Elvidge et al. (2015) examined the features of light fishing boats and noted that they are generally spikes. Moreover, they presented an algorithm for the automatic detection of spikes to extract boat pixels based on VIIRS DNB data. Similarly, Cozzolino and Lasta (2016) proposed an alternative algorithm that combined a set of standard techniques for digital image processing (enhancement, thresholding, and segmentation) to detect lights from ships based on DNB data. Straka et al. (2015) highlighted the improved ability of the DNB to observe ship lights by exploring three illustrative case studies. Therefore, this set of data has great potential for the quantitative monitoring of light seine fishing vessels (Elvidge et al. 2013; Guo et al. 2017).

In this study, we performed large-scale spatial analyses to quantitatively and qualitatively evaluate variations in the potential light seine fishing areas in the East China Sea based on VIIRS DNB images. Specifically, to investigate the characteristics of light seine fishing in the East China Sea, fishing vessel pixels were detected based on the research of (Elvidge et al. 2015). Additionally, hotspots of light seine fishing areas were detected using cluster analysis. More specific geographic features of these hotspots were further explored using various geographic tools, including the grey weighted method, standard deviational ellipse (SDE), concave hull, and kernel density. The results of this study provide reliable information concerning where and when light seine fishing occurs and suggest that VIIRS DNB imagery can be used to effectively detect light seine fishing areas.

2. Study area and data processing

2.1. *Study area*

The East China Sea is one of the most important fishing areas in China and encompasses approximately 0.7 million square kilometres. The average water depth of the sea is 1000 m. This area is located to the east of China's mainland, south of South Korea, and west of the Japanese mainland. The Yellow Sea is on the northern side of the East China Sea, and the South China Sea is on the southern side. The main extent of the East China Sea lies between [119.13 E, 33.28 N] and [131.08 E, 24.05 N] (Organization, International Hydrographic 1953).

The East China Sea has a vast continental shelf and flat seabed. The water is of high quality, with many types of water masses meeting there that provide good breeding, feeding, and overwintering conditions for various fish species. Thus, high-quality fishing areas are formed. Light seine fishing is one of the major operating methods in this area, and the main fishing period is from July to September (Zheng 2008), with a fishing moratorium on light seine fishing enacted from May 1st to July 1st in recent years (according to The Ministry of Agriculture of the People's Republic of China).

2.2. *Data sources and processing*

2.2.1. *Data sources*

The data used in this study mainly include VIIRS nighttime light data. The VIIRS on the S-NPP satellite is part of a joint mission between NASA's Earth Observing System (EOS) and the Joint Polar-Orbiting Satellite System (JPSS), which was first launched on 28 October 2011 (Lee et al., 2010; Hillger et al., 2013). In this study, the monthly DNB cloud-free composites were employed to detect fishing vessels (www.ngdc.noaa.gov/eog/viirs/download_dnb_composites.html). The data set is produced by calculating the average radiance of each DNB pixel for the entire month, which is a statistically meaningful approach for detecting fishing areas. Because fishing areas are relatively stable in certain periods, monthly images reflect the frequency of fishing vessels in certain areas rather than the presence of a single vessel. High DNB values correspond to a greater number of fishing vessels and a greater quantity of fish. This data set has been filtered to exclude data impacted by stray light, lighting, lunar illumination, and cloud cover. However, lights from auroras, fires, vessels, and other temporal sources are retained, and such anomalies are inconsistent with the records in the DMSP-OLS data sets. According to NOAA's production description, the VIIRS DNB dataset has two configurations denoted as 'vcmcfg' and 'vcmslcfg'. The 'vcmslcfg' version, which includes stray light-corrected data, has more data coverage toward the poles but is of reduced quality. Thus, the 'vcmcfg' configuration, which is of better quality, was selected as the data source in this study.

The spatial resolution of the data set was approximately 15 arc seconds, which is much better than that of the DMSP-OLS data set. The monthly imagery was divided into six tiles, and each tile was bound by the equator and spanned a longitude of 120°. The images covering the East China Sea were stored in the 'tile 3 (75N/060E)' data set on the website, and the study period was from March 2012 to December 2016.

2.2.2. *Data processing*

When detecting fishing areas using DNB images, regions of interest for selection may include fires, volcanoes, auroras, vessels, and other temporal features. Pixels with high DNB radiance from vessels indicate a greater possibility of representing a fishing area pixel. In this study, the proposed fishing area detection method is based on the research of Elvidge et al. (Elvidge et al. 2015b). The detailed processing flow is shown in Figure 1. Three main indicators, including the spike median index (SMI), sharpness index (SI) and spike height index (SHI), were calculated to identify the real fishing area pixels. Key threshold values were determined by experiments, and two criteria were used to define one fishing area pixel: (1) SMI> 0.035, SI> 0.4, and 0.75< SHI< 0.995 or (2) SMI> 0.035, SI> 0.4, SHI> 0.995, and DNB radiance <1000. The detailed processes are listed below.

(1) Data preprocessing

The study data were extracted from the monthly data set of the East China Sea. To avoid the impacts of light from the mainland and islands, a 20-km buffer zone was configured. A logarithmic transformation of the DNB values was applied to enhance the contrast among features. Thus, the data set consisted of pixels with $\log_{10}$(DNB) values.

(2) Spike median index (SMI)

The SMI was calculated as follows:

$$\mathrm{SMI} = P_{i,j} - P_{i,j}{}' \tag{1}$$

where $P_{i,j}$ represents the $\log_{10}$(DNB) of a pixel in row i and column j and $P_{i,j}{}'$ represents the grey value of a pixel in row i and column j processed with a 3 × 3 pixel median filter.

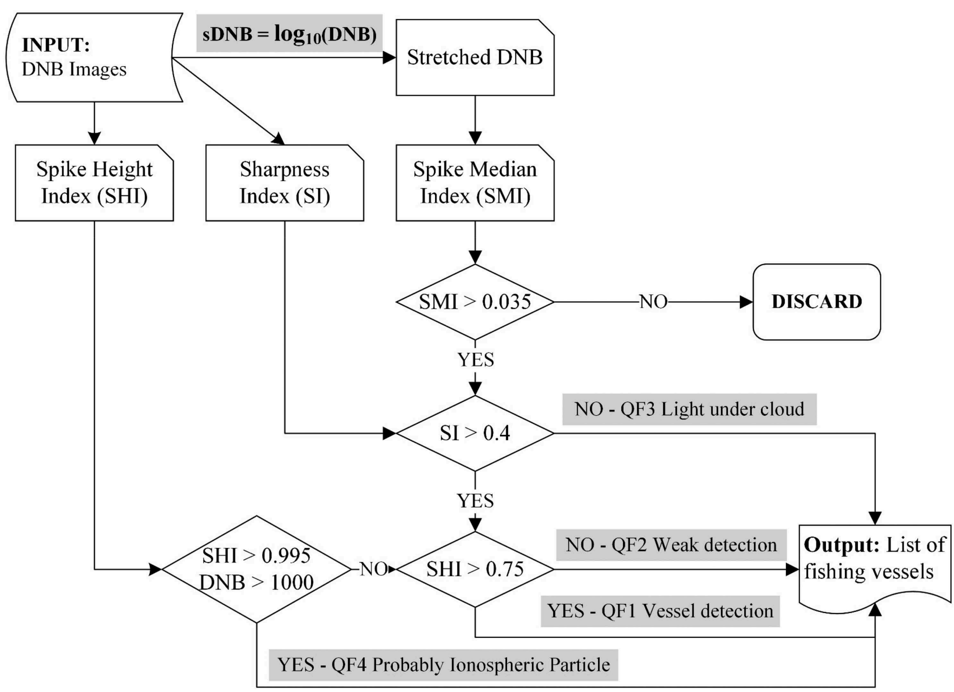

Figure 1. Processing flow chart for VIIRS boat detection under low lunar illuminance conditions.

We selected 0.035 as the threshold of the SMI. Thus, pixels with SMI values greater than 0.035 were considered to represent a spike.

(3) Sharpness index (SI)

To differentiate obscured pixels, we used the image SI to evaluate the original image. Elvidge et al. used the S3 algorithm in many experiments (Elvidge et al. 2015a; Vu, Phan, and Chandler 2012) and distinguished between fuzzy and clear SMI detection results with a threshold of 0.4. Similarly, clear detection results with SI values greater than 0.4 were obtained in this study.

(4) Spike height index (SHI)

To distinguish between high-energy particles, weak detection results and strong detection results (fishing boats), Elvidge et al. applied the SHI (Elvidge et al. 2015a).

$$\mathrm{SHI} = \frac{(P_{i,j} - P_{\mathrm{avg\_adj}})}{P_{i,j}} \tag{2}$$

$$P_{\mathrm{avg\_adj}} = \min\{P_{\mathrm{horizontal}}, P_{\mathrm{vertical}}\} \tag{3}$$

$$P_{\mathrm{horizontal}} = \frac{P_{i,j-1} + P_{i,j+1}}{2}, P_{\mathrm{vertical}} = \frac{P_{i-1,j} + P_{i+1,j}}{2} \tag{4}$$

where $P_{i,j}$ represents the grey value of a pixel in row i and in column j, $P_{\mathrm{avg_adj}}$represents the average radiance of two adjacent pixels. The pixels with SHI values greater than 0.75 were retained.

3. Methods

Based on the fishing vessel detection process proposed in the previous section, a series of fishing area data sets was extracted from April 2012 to December 2016 and used to conduct a spatiotemporal pattern analysis of the fishing areas in the East China Sea. Table 1 shows the statistical count of fishing vessel pixels detected from each monthly DNB data set.

A significance test (Farris et al., 1995) was conducted to verify the results for fishing vessel pixel detection based on Table 1. Each column represents a sample from the population that indicates the actual fishing vessel pixel count. If significant differences

Table 1. Fishing vessel pixel count from 2012 to 2016.

Year / Month	Fishing Vessel Pixel Count				
	2012	2013	2014	2015	2016
1	N/A	438	331	388	388
2	N/A	157	184	75	172
3	N/A	315	273	242	196
4	408	456	202	195	175
5	473	365	304	414	385
6	382	541	377	542	580
7	3467	4112	3283	1819	2956
8	2862	3544	3119	2068	2485
9	1568	3113	1286	2355	1406
10	1076	1096	1212	1337	1131
11	1072	966	1256	813	595
12	856	826	314	619	719

are not observed among the populations from which the samples were obtained, then the results are more likely to be true. In this study, the Friedman test (Sheldon, Fillyaw, and Thompson 2010), which is a non-parametric statistical test that provides a measure of difference between paired groups by rank, was used. The null hypothesis of the test is that 'significant differences would occur across the population'. To confirm the accuracy of the result of fishing vessel detection, the null hypothesis must be accepted based on the samples. In general, without drastic changes in natural factors or government policies for fishery management, fishing activities should proceed normally. Therefore, the fishing vessel pixel patterns are likely consistent without significant differences. We used R to execute the Friedman test, and the data in Table 1 were divided into two data sets because the test requires a matching number of data sets. The first data set consisted of the fishing vessel pixel count from January to December between 2013 and 2016, and the second consisted of the pixel count from April to December between 2012 and 2016.

3.1. *Cluster pattern of fishing areas at multiple spatial scales*

In the first part of the spatiotemporal analysis, cluster pattern analysis was applied to identify hotspots of light seine fishing areas. As stated above, a large number of fishing vessel pixels represents a high probability that the area is a fishing area. Therefore, the sea areas where lots of fishing vessel pixels gather could be fishing areas. To extract the spatial pattern of these hotspots, the unweighted Ripley's *K*-Function was used. Ripley's *K*-Function is a type of estimator used to describe the correlations among objects in a given field and can describe the characteristics of point processes at many distance scales (Dixon and Philip 2006). This indicator was used to determine the overall distribution trend (clustered or dispersed) of light seine fishing areas in the East China Sea.

Ripley's *K*-Function can be described as follows:

$$L(d) = \sqrt{\frac{A \sum_{i=1}^{n} \sum_{j=1, j \neq i}^{n} k_{i,j}}{\pi n(n-1)}} \tag{5}$$

where d is the distance, n is equal to the total number of features, A represents the total area of the features and $k_{i,j}$ is a weight. If there is no edge correction, then the weight will equal one when the distance between i and j is less than d and will equal zero otherwise.

According to the results of Ripley's *K*-Function, the fishing areas in all months were not dispersed and instead distributed as clusters. Therefore, cluster analysis using the DBSCAN (density-based spatial clustering of applications with noise) method (Idrissi and Alaoui 2016) was conducted to obtain the clustering pattern. The DBSCAN algorithm was developed to identify arbitrarily shaped clusters based on the spatial data density, and a cluster can be recognized if the spatial point density of a region exceeds a certain threshold. To use this approach, two main variables must be clarified (Ester et al., 1996): (1) ϵ (eps), which defines the distance threshold of a neighbouring region, and (2) minPts, the minimum number of points required to form a dense region. To identify the optimal ϵ value, the k-nearest neighbourhood distance matrix was used, and the

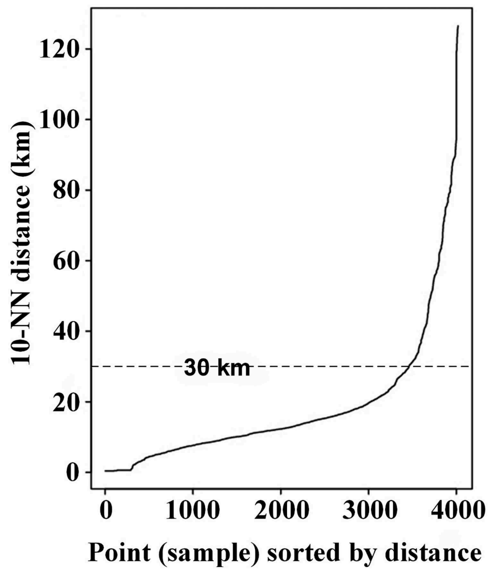

Figure 2. Plot of the k-nearest neighbourhood distance for fishing vessel pixels in April 2012.

fishing vessel pixels were extracted as point features in a vector model. Then, the function kNN distplot in the DBSCAN package was used to obtain the k-distance pattern and identify the optimal ϵ value. To identify the optimal minPts value, the number of points within the ϵ radius of each point in the data set was calculated. Then, minPts was obtained from the mathematical expectation of all the calculated points. According to our experiments for all months, the optimal ϵ value was 30 km, and the optimal minPts value was 10. One of the months (April 2012) was selected to show the optimal value of ϵ, which is indicated by the inflection point along the k-distance curve (Figure 2).

3.2. *Barycenter of fishing areas*

The specific geographic features of the identified fishing hotspots were further explored. The geometric barycenter of each fishing area (April 2012 to December 2016) was calculated by the grey weighted method (Lehodey et al., 1997), in which each point was assigned a weight based on the associated grey value. The barycenter reflects the general movement of the potential light seine fishing areas in the East China Sea.

$$\bar{X} = \frac{\sum_{i=1}^{n}(P_i \times x_i)}{\sum_{i=1}^{n} P_i}, \bar{Y} = \frac{\sum_{i=1}^{n}(P_i \times y_i)}{\sum_{i=1}^{n} P_i} \tag{6}$$

where $\bar{X}$ and $\bar{Y}$ represent the longitude and latitude of the barycenter of the fishing ground in a certain month, respectively; x_i and y_i represent the longitude and latitude of the i^{th} fishing vessel pixel; P_i represents the grey value of the i^{th} fishing vessel pixel; and n is the total number of fishing vessel pixels in each month.

3.3. *Fishing area ranges and directions*

The SDE method is a classical algorithm used to measure the direction and distribution of a point data set and was first proposed by Lefever (Lefever 1926) in 1926, and it was used to determine the main trend in orientation of fishing areas and the significance of the trend. It is assumed that the fishing vessel pixels obeyed a normal distribution; therefore, the SDE with two standard deviations was used to reduce the impact of abnormal pixels. Approximately 95.4% of the fishing vessel pixels were distributed in the range of twice the standard deviation (Pixels beyond this range were considered exceptions). In addition, to calculate the area of the fisheries, a polygon was created via a concave hull method based on the pixels, and the area of the polygon is considered the fishery area after the removal of abnormal pixels.

The SDE direction is calculated as follows:

$$\tan\theta = \frac{\left(\sum_{i=1}^{n}\widetilde{x}_i^{2} - \sum_{i=1}^{n}\widetilde{y}_i^{2}\right) + \sqrt{\left(\sum_{i=1}^{n}\widetilde{x}_i^{2} - \sum_{i=1}^{n}\widetilde{y}_i^{2}\right)^{2} + 4\left(\sum_{i=1}^{n}\widetilde{x}_i\widetilde{y}_i\right)^{2}}}{2\sum_{i=1}^{n}\widetilde{x}_i\widetilde{y}_i} \tag{7}$$

where θ is the angle from the north direction to the long axis of the ellipse, indicating the main trend in the orientation of the fishing areas, $\widetilde{x}_i$ and $\widetilde{y}_i$ represent the deviation of *xy* coordinates from the average centre of fishing area, n is the total number of fishing vessel pixels in a certain month and i represents the sequence number of the pixel.

Then, ellipticity of the SDE was calculated as follows to reflect the significance of the trend in orientation of the fishing area:

$$O = \frac{a-b}{a} \tag{8}$$

where O is the ellipticity of SDE, a is the length of the major semi axis, b is the length of the minor semi axis.

A concave hull is a polygon that more precisely illustrates the area occupied by point data versus that based on a convex hull. In general, the concave hull area of a point data set is smaller than that of a convex hull. To obtain a more accurate fishery area, the isolated fishing vessel pixels were not considered when constructing the concave hull, and subpolygons were generated according to the cluster pattern of fishing vessel pixels to avoid inflated area values. Figure 3 shows the concave hulls of the data set in April and July 2012.

3.4. *Fishing vessel pixel density*

The density of fishing areas was explored because it can effectively reflect the internal differences among fishing hotspots. We used the kernel density tool in ArcGIS 10.2 to analyse the density distribution of fishing vessel pixels. This tool calculates the density of a feature based on its surrounding neighbourhood and can be applied to both points and lines. We used the tool with points in this study. In contrast to the ordinary density analysis tool, the points that fall into the search area have different weights. Specifically, the points near the search centre are assigned high weights, and the distribution of

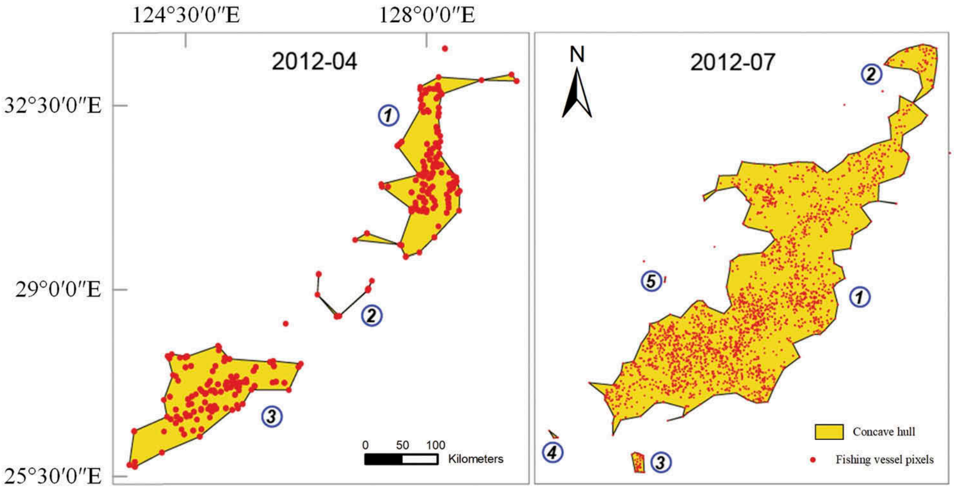

Figure 3. Concave hull of the fishing vessel pixels in April and July of 2012.

results is relatively smooth. A continuous surface can typically be generated based on the points.

The kernel function, which is the core function of the kernel density tool, is based on the four-core function described by Silverman (B.W. Silverman 1986).

$$K_2(x) = \begin{cases} 3\pi^{-1}(1 - x^T x)^2, (if\ x^T x < 1) \\ 0, (\text{otherwise}) \end{cases} \tag{9}$$

where T is the mathematical operator that represents the transpose of matrix.

4. Results and discussion

4.1. *Fishing vessel detection and verification*

The fishing vessel pixels from April 2012 to December 2016 were extracted (Figure 4). We counted all fishing vessel pixels in the results, which are presented in Table 1. The Friedman test results of the first data set (January to December between 2013 and 2016) are as follows: *chi-squared* = 4.36, *df* = 3, and $p = 0.225 > 0.05$. The null hypothesis was accepted, and significant differences were not observed among the populations. The Friedman test results of the second data set (April to December between 2012 and 2016) are as follows: *chi-square* = 3.93, *df* = 3, and $p = 0.268 > 0.05$. The null hypothesis was again accepted, and significant differences were not observed among the populations. These results indicate that the detection results are of satisfactory accuracy.

The change in the number of fishing vessel pixels is shown in Figure 5. Regularity can be observed over time. Notably, fewer pixels and slight fluctuations appear between January and June, and a sudden dramatic increase is observed from June to July. Then, the number of detected pixels gradually decreases and returns to a lower level at the end of the year.

As noted in section 3, a fishing moratorium on light seine fishing offshore in China has been enacted annually from May 1st to July 1st in recent years. During this time, no

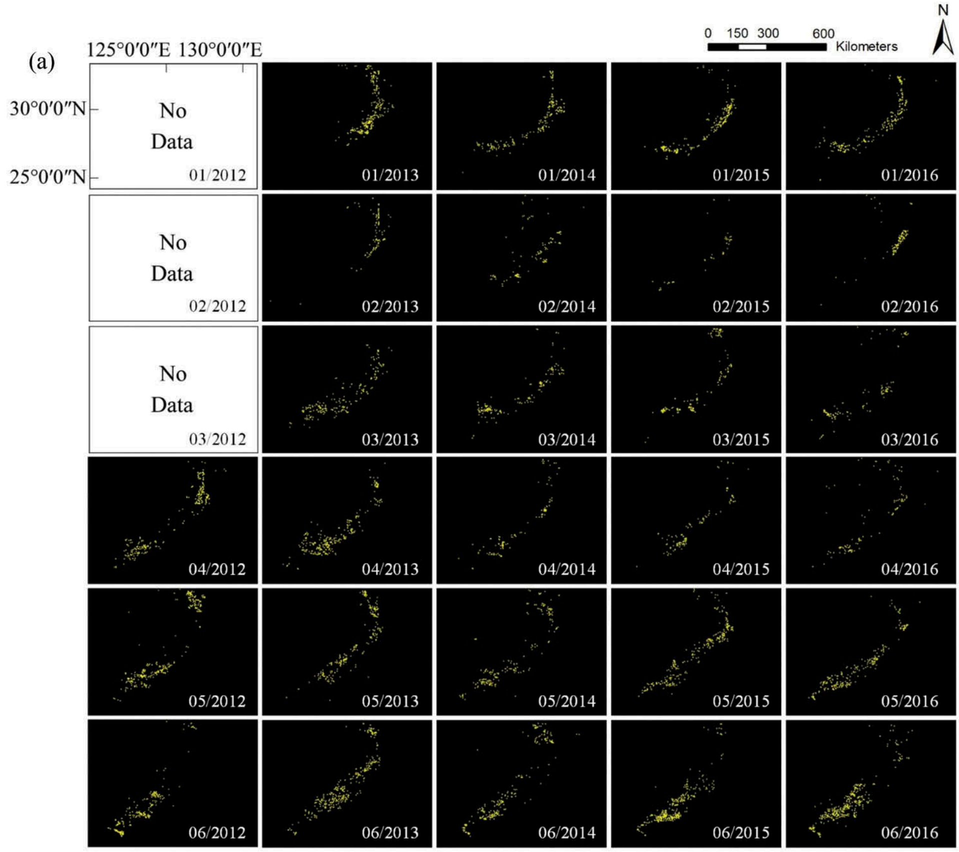

Figure 4a. Fishing vessel detection results from (a) January to June and (b) July to December between 2012 and 2016 (yellow points represent the detected fishing vessel pixels).

light seine fishing boats are allowed to leave the port. The end of the fishing moratorium on July 1st contributes to the dramatic increase in light seine fishing, as confirmed by the trend of the quantity of vessel pixels.

4.2. *Cluster pattern analysis of the fishing areas*

The cluster pattern reflects the distribution of light seine fishing hotspots (Figure 6). A similar pattern with an initial concentration and then decentralization is observed from 2012–2016.

Specifically, the light seine fishing vessels are dispersed without large clusters from February to April. From the end of April to the beginning of May, the population begins to increase with the beginning of spawning activities. The fish affected by the Kuroshio Front move northward with the emergence of some nascent fishing areas. From May to June, the scale of light seine fishing is limited because of the fishing moratorium. In July and August, the population begins to exhibit explosive growth after two months of fishing moratorium, with a high concentration of light seine fishing vessels in the area.

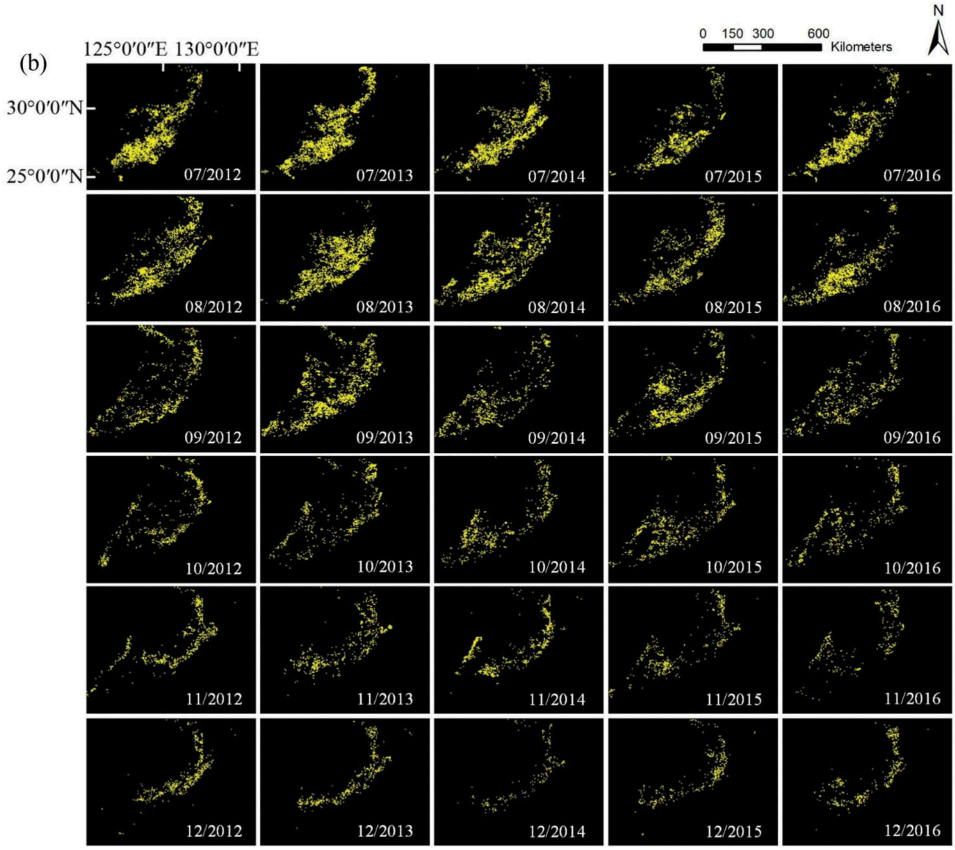

Figure 4b. (Continued.)

Large-scale fishing areas are distributed in the northeast to southwest direction in the East China Sea. In September, the population of fish decreases significantly after two months of high-intensity fishing, and large-scale fishing areas become scattered and form many small-scale fisheries in the southwestern and northeastern East China Sea. The scattered fishing areas also display a continuous decline in scale. This trend continues until April of the following year, forming almost random fishing areas that combine again in May.

An interannual analysis shows that the scale of the fishing areas has been continually declining in recent years. The decline reflects a reduction in fishery resources in the East China Sea, which should draw the attention of relevant resource management departments.

4.3. *Variations in the fishing area barycenter*

The latitude and longitude of the fishing area barycenter are counted separately (Figure 7). The barycenter is relatively evenly distributed between 123.5°E ~ 127.5°E and 27°N ~ 30.5°N. The overall trends of latitude and longitude are similar: first

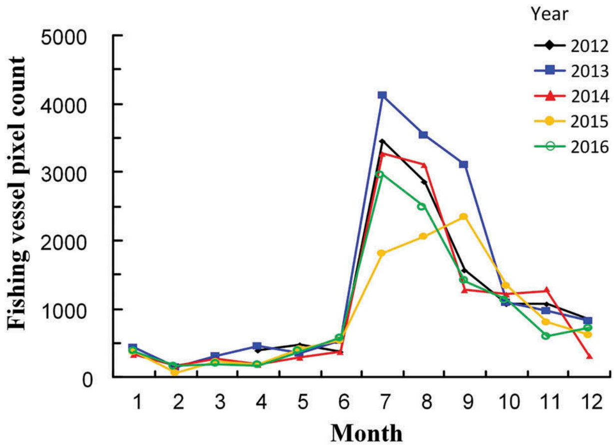

Figure 5. Monthly variation in the fishing vessel pixel count.

decreasing and then increasing, reaching a minimum in the middle of the year, and returning to the original level at the end of the year. This pattern suggests that the barycenter moves from the northeast to southwest and then northeast during the year. To further analyse this pattern, the barycenter data were averaged in each month (January to December), and the five-year average (2012–2016) barycenter was obtained (Figure 8).

The fishing area barycenter displays opposite movement trends in the first half and second half of the year. In latitude, the barycenter moved from 29.30°N in January to 28.07°N in June and then to 29.43°N in December (from east to west to east), with a fluctuation of approximately 1.3°. In longitude, the barycenter moved from 126.37°E in January to 124.49°E in June and then to 126.15°E in December (from north to south to north), with a fluctuation of approximately 1.8°. The movement of fishing area barycenter can be closely linked with changes in the SST (SST results can be downloaded from https://oceancolor.gsfc.nasa.gov/). Taking the year 2013 as an example, in spring and summer (March to August), as the water temperature increased, the fishing vessel groups gradually move southwest. In contrast, in autumn and winter (September to February) when the water temperature decreases, the fishing vessel groups gradually move in the opposite direction (northeast). This phenomenon reflects the impacts of water temperature changes on light seine fishing and the distribution of fisheries.

In addition, obvious seasonal agglomeration can be observed in the fishing areas. The barycenter is centrally distributed in the winter (approximately 29.4°N, 126.5°E), spring (approximately 28.6°N, 125.3°E) and summer (approximately 28.3°N, 124.6°E). However, in autumn (September to November), the barycenter moves northeast, with a variation close to 1° in both longitude and latitude.

4.4. *Range and direction analysis of fishing areas*

The concave hull area was applied to represent the range of the light seine fishing area in each month. In general, the area expands first and then decreases. Additionally, it is

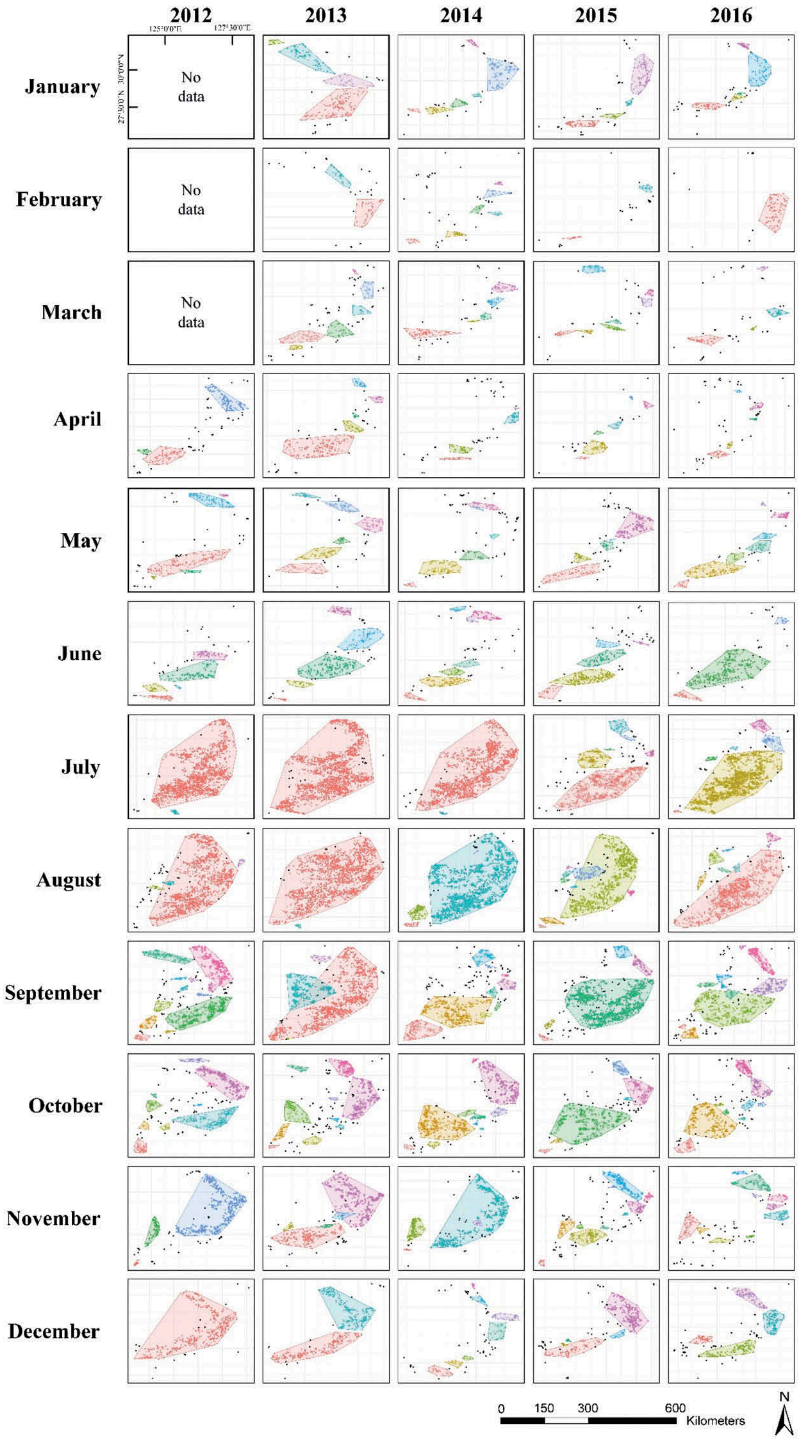

Figure 6. Cluster pattern variations from January to December in 2012–2016.

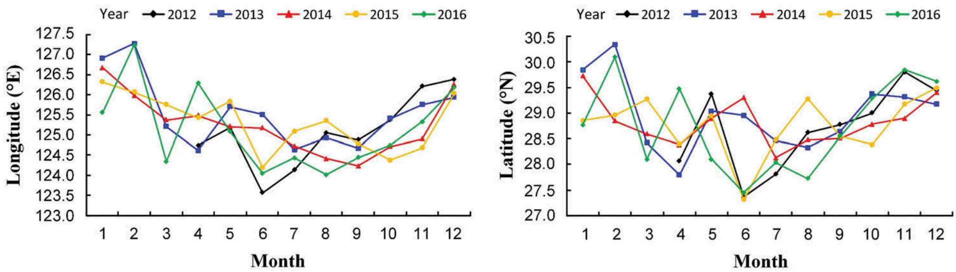

Figure 7. Monthly change in the latitude and longitude of the fishing area barycenter.

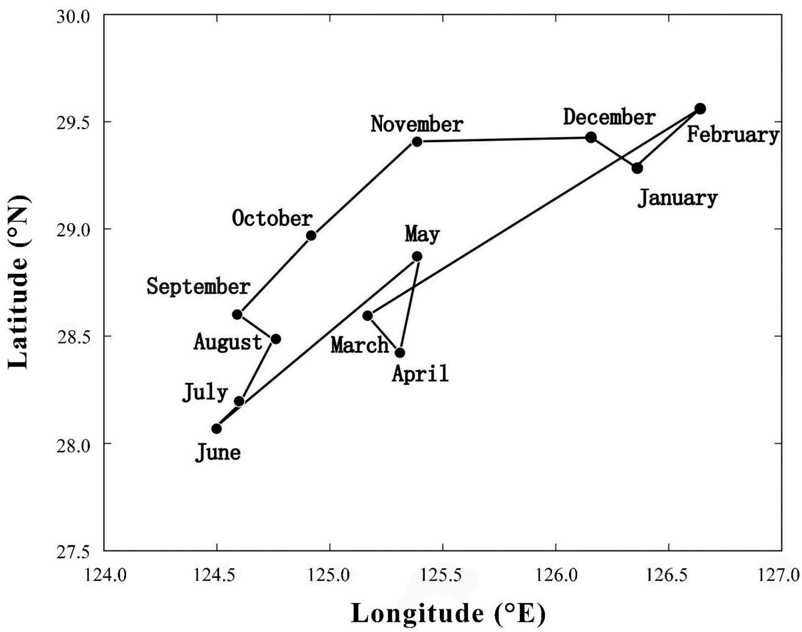

Figure 8. Monthly five-year average fishing area barycenter.

striking that the peak month has advanced from September to August since 2014; specifically, the peak area value in Figure 9a appears in September in 2012 and 2013 and in August between 2014 and 2016, accompanied by an obvious decrease in the peak value. Both trends reflect the increased shortage of fishery resources.

The direction of the SDE was applied to represent the trend in the orientation of the fishing areas (Figure 9b). Taking the north direction as the starting axis, nearly all azimuths are distributed between 30° and 50°, and the oblateness of the SDE is generally greater than 0.6 (reaching 0.8). This finding suggests that the distribution of fishing areas exhibits a strong tendency in orientation. This trend may be correlated with marine factors. In fact, this type of distribution is highly consistent with the direction of the Kuroshio Front in the East China Sea, which is a well-known warm oceanic western boundary current that can affect the temperature and salinity of the ocean. In the past, a significant relationship has been observed between the Kuroshio Front and the

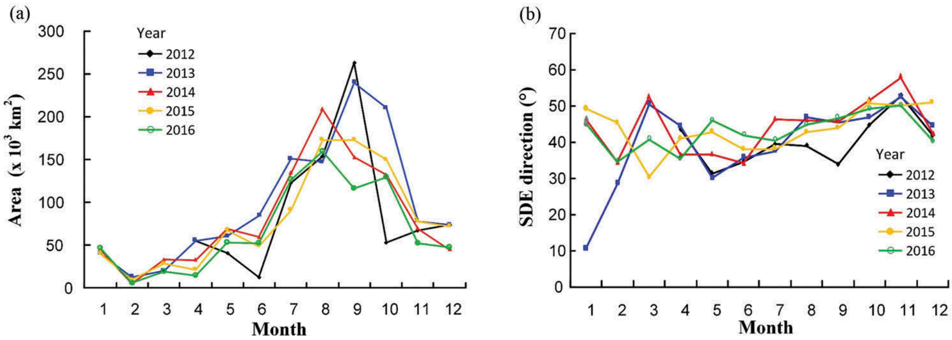

Figure 9. Monthly variation in the (a) concave hull area and (b) SDE direction.

hydrographic and fishery conditions in the East China Sea (Lie and Cho 2002), which indicates a close connection between the Kuroshio Front and fishing areas in this study region.

4.5. *Density analysis of fishing areas*

The density analysis results reflect the target areas and optimal times for light seine fishing (Figure 10). Over the year, the density of light seine fishing is highest in summer (July and August). Compared with the fishing activity in other seasons, fishing in summer occurs over larger areas and in more concentrated clusters. Furthermore, the fishing intensity in the second half of the year is much greater than that in the first half. These fishing patterns are consistent with the main period of light seine fishing in this area (Zheng 2008).

Interannual density analysis reveals that the fishing intensity decreases annually during the study period. The decline may be correlated with the Chinese government's regulations on fishing in the East China Sea. The fishing moratorium on offshore light seine fishing in China was adjusted to the period from May 1st to August 1st in 2017 (May 1st to July 1st before 2017) (www.moa.gov.cn/govpublic/YYJ/201701/t20170120_5460478.htm), which reflects a more stringent fishing policy.

In addition, the concave hulls were stacked (obtained in section 3.3) to count the number of layers in each pixel, which reflects the fishing frequency in the East China Sea over time (Figure 11). The results show that high-frequency areas are continuously distributed, with many located in the southern portion of the study area.

5. Conclusions

In this study, VIIRS DNB imagery data were used to identify the spatiotemporal patterns of potential light seine fishing areas in the East China Sea. The fishing vessel pixels were detected as described by Elvidge et al. Then, the spatiotemporal patterns of the fishing areas were explored from four perspectives: cluster pattern analysis at multiple spatial scales, the calculation of the fishing area barycenter, analyses of range and direction, and an analysis of the fishing area density. Compared with previous studies of fishing

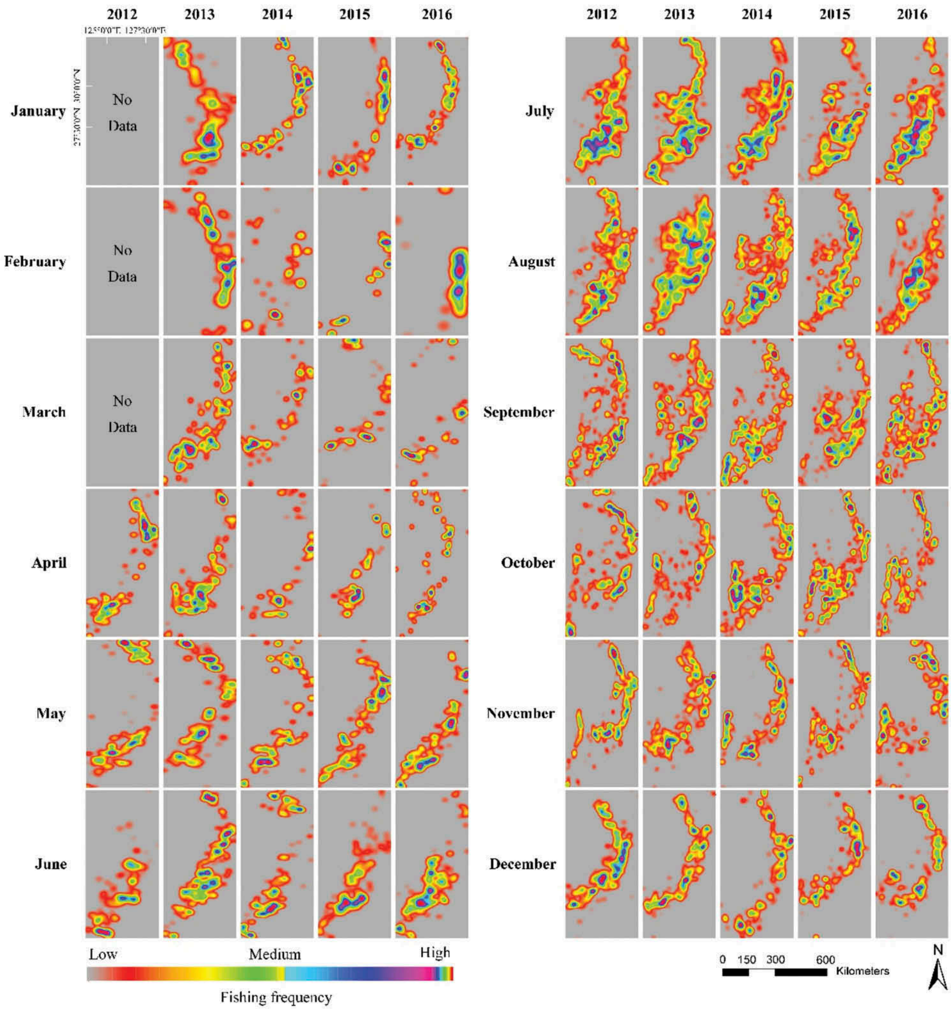

Figure 10. Results of the density analysis from January to December between 2012 and 2016.

areas, nighttime light images provide a more effective approach for the large-scale analysis of spatiotemporal pattern changes. Moreover, this technique can be expanded to similar studies in other areas because of the global scope of the imagery. This study provides reliable information concerning where and when light seine fishing occurs. In addition, the results demonstrate that VIIRS DNB imagery can be effectively used to detect light seine fishing areas and has the potential to play a role in establishing long-term fishery resource regulations and combating illegal, unregulated, and unreported (IUU) fishing activities.

Although the results of the spatiotemporal analysis in this study are in good agreement with the results of other scholars, only a single band of the VIIRS images was applied. Therefore, the information obtained here is limited, and the boat identification results may also contain errors. Moreover, different types of light fishing vessels cannot be distinguished. In the future, determining how to improve the identification accuracy of fishing vessels and even distinguish between different types of vessels are worth exploring.

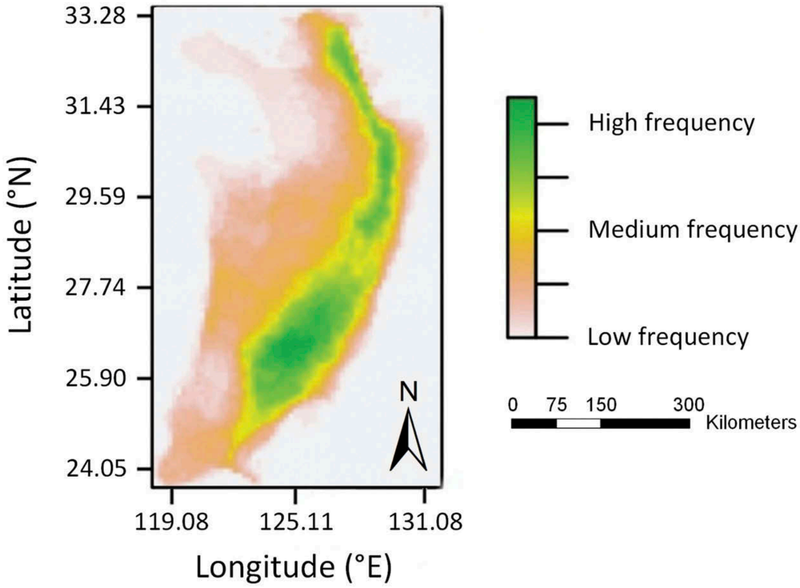

Figure 11. Fishing frequency in the East China Sea (2012–2016).

Disclosure statement

No potential conflict of interest was reported by the authors.

Funding

This research was financially supported by the National Key R&D Program of China [2017YFB0503500].

References

Berkeley, S., M. Hixon, R. Larson, and M. Love. 2004. "Fisheries Sustainability via Protection of Age Structure and Spatial Distribution of Fish Populations." *Fisheries* 29 (8): 23–32. doi:10.1577/1548-8446(2004)29[23:FSVPOA]2.0.CO;2.

Chang, Y. J., C. L. Sun, Y. Chen, S. Z. Yeh, and G. Dinardo. 2012. "Habitat Suitability Analysis and Identification of Potential Fishing Grounds for Swordfish, Xiphias Gladius, in the South Atlantic Ocean." *International Journal of Remote Sensing* 33 (23): 7523–7541. doi:10.1080/01431161.2012.685980.

Chen, Q. X., Z. Y. Xiong, W. Q. Shi, and J. Y. Peng. 2013. "A Preliminary Study on the Phototaxis of Horse Mackerel (Trachurus Japonicas) and Amberfish (Decapterus Maruadsi)." *Advanced Materials Research* 647: 210–213. doi:10.4028/www.scientific.net/AMR.647.210.

Chen, X., L. Gang, B. Feng, and S. Tian. 2009. "Habitat Suitability Index of Chub Mackerel (Scomber Japonicus) from July to September in the East China Sea." *Journal of Oceanography* 65 (1): 93–102. doi:10.1007/s10872-009-0009-9.

Cho, K., R. Ito, H. Shimoda, and T. Sakata. 1999. "Technical Note and Cover Fishing Fleet Lights and Sea Surface Temperature Distribution Observed by DMSP/OLS Sensor." *International Journal of Remote Sensing* 20 (1): 3–9. doi:10.1080/014311699213569.

Choi, K., C. I. Lee, K. Hwang, S. W. Kim, J. H. Park, and Y. Gong. 2008. "Distribution and Migration of Japanese Common Squid, Todarodes Pacificus, in the Southwestern Part of the East (Japan) Sea." *Fisheries Research* 91 (2): 281–290. doi:10.1016/j.fishres.2007.12.009.

Cole, J., and C. Villacastin. 2000. "Sea Surface Temperature Variability in the Northern Benguela Upwelling System, and Implications for Fisheries Research." *International Journal of Remote Sensing* 21 (8): 1597–1617. doi:10.1080/014311600209922.

Cozzolino, E., and C. A. Lasta. 2016. "Use of VIIRS DNB Satellite Images to Detect Jigger Ships Involved in The Illex Argentinus Fishery." *Remote Sensing Applications: Society and Environment* 4: 167–178.

Dixon, D., and M. Philip. 2006. *Ripley's K Function*. John Wiley & Sons.

Elvidge, C., M. Zhizhin, K. Baugh, and F. C. Hsu. 2015. "Automatic Boat Identification System for VIIRS Low Light Imaging Data." *Remote Sensing* 7 (3): 3020–3036. doi:10.3390/rs70303020.

Elvidge, C. D., K. E. Baugh, M. Zhizhin, and F. C. Hsu. 2013. "Why VIIRS Data are Superior to DMSP for Mapping Nighttime Lights." *Proceedings of the Asia-Pacific Advanced Network* 35: 62–69. doi:10.7125/APAN.35.7.

Ester, M., H. -P. Kriegel, J. Sander, and X. Xu. 1996. A Density-based Algorithm for Discovering Clusters in Large Spatial Databases with Noise. I*nternational conference on Knowledge Discovery and Data Mining (KDD-96)*.

Farris, J. S., M. Kallersjo, A. G. Kluge, and Carol Bult. 1995. "Constructing a Significance Test for Incongruence." *Systematic Biology* 44 (4): 570–572.

Gauthierouellet, M., M. Dionne, F. Caron, T. L. King, and L. Bernatchez. 2009. "Spatiotemporal Dynamics of the Atlantic Salmon (Salmo Salar) Greenland Fishery Inferred from Mixed-Stock Analysis." *Canadian Journal of Fisheries & Aquatic Sciences* 66 (12): 2040–51(12). doi:10.1139/F09-147.

Guo, G., F. Wei, J. Xue, S. Zhang, H. Zhang, F. Tang, and T. Cheng. 2017. "Identification for Operating Pelagic Light-Fishing Vessels Based on NPP/VIIRS Low Light Imaging Data." *Transactions of the Chinese Society of Agricultural Engineering* 33 (10): 245–251.

Hillger, D., T. Kopp, T. Lee, D. Lindsey, C. Seaman, S. Miller, and J. Solbrig et al. 2013. ""First-light Imagery from Suomi NPP VIIRS. " *Bulletin Of the American Meteorological Society* 94 (7): 1019–1029.

Idrissi, A., and A. Alaoui. 2016. "A Multi-criteria Decision Method in The DBSCAN Algorithm for Better Clustering." *International Journal of Advanced Computer Science and Applications* 7 (2): 377–384.

Kiyofuji, H., S. Saitoh, Y. Sakurai, T. Hokimoto, and K. Yoneta. 2001. "Spatial and Temporal Analysis of Fishing Fleet Distribution in the Southern Japan Sea in October 1996 Using DMSP/OLS Visible Data." *Anesthesia & Analgesia* 83 (4): 878–879.

Kiyofuji, H., and S. I. Saitoh. 2004. "Use of Nighttime Visible Images to Detect Japanese Common Squid Todarodes Pacificus Fishing Areas and Potential Migration Routes in the Sea of Japan." *Marine Ecology Progress* 276 (1): 173–186. doi:10.3354/meps276173.

Kumari, B., and M. Raman. 2010. "Whale Shark Habitat Assessments in the Northeastern Arabian Sea Using Satellite Remote Sensing." *International Journal of Remote Sensing* 31 (2): 379–389. doi:10.1080/01431160902893444.

Lee, T. F., C. S. Nelson, P. Dills, L. P. Riishojgaard, A. Jones, L. Li, and S. Miller et al. 2010. "NPOESS: Next-generation Operational Global Earth Observations." *Bulletin Of the American Meteorological Society* 91 (6): 727–740.

Leeney, R. H., A. C. Rachel Amies, M. J. Broderick, J. L. Witt, J. Doyle, and B. J. Godley. 2008. "Spatio-Temporal Analysis of Cetacean Strandings and Bycatch in a UK Fisheries Hotspot." *Biodiversity & Conservation* 17 (10): 2323. doi:10.1007/s10531-008-9377-5.

Lefever, D. W. 1926. "Measuring Geographic Concentration by Means of the Standard Deviational Ellipse." *American Journal of Sociology* 32 (1): 88–94. doi:10.1086/214027.

Lehodey, P., M. Bertignac, J. Hampton, A. Lewis, and J. Picaut. 1997. "El Nin˜o Southern Oscillation and Tuna in The Western Pacific." *Nature* 389 (6652): 715–718.

Li, D., and X. Li. 2015. "An Overview on Data Mining of Nighttime Light Remote Sensing." *Acta Geodaetica Et Cartographica Sinica* 44 (6): 591–601.

Li, G., J. Cao, X. Zou, X. Chen, and J. Runnebaum. 2016. "Modeling Habitat Suitability Index for Chilean Jack Mackerel (Trachurus Murphyi) in the South East Pacific." *Fisheries Research* 178: 47–60. doi:10.1016/j.fishres.2015.11.012.

Li, G., X. Chen, L. Lei, and W. Guan. 2014. "Distribution of Hotspots of Chub Mackerel Based on Remote-Sensing Data in Coastal Waters of China." *International Journal of Remote Sensing* 35 (11–12): 4399–4421. doi:10.1080/01431161.2014.916057.

Lie, H. J., and C. H. Cho. 2002. "Recent Advances in Understanding the Circulation and Hydrography of the East China Sea." *Fisheries Oceanography* 11 (6): 318–328. doi:10.1046/j.1365-2419.2002.00215.x.

Maravelias, C. D., D. G. Reid, and G. Swartzman. 2000. "Seabed Substrate, Water Depth and Zooplankton as Determinants of the Prespawning Spatial Aggregation of North Atlantic Herring." *Marine Ecology Progress* 195 (1): 249–259. doi:10.3354/meps195249.

Marttila, M., K. Kyllönen, and T. P. Karjalainen. 2016. "Social Success of In-Stream Habitat Improvement: From Fisheries Enhancement to the Delivery of Multiple Ecosystem Services." *Ecology & Society* 21: 1. doi:10.5751/ES-08118-210104.

Organization, International Hydrographic. 1953. Limits of Oceans and Seas. Paper presented at the AGU Fall Meeting.

Paulino, C., M. Segura, and C. German. 2016. "Spatial Variability of Jumbo Flying Squid (Dosidicus Gigas) Fishery Related to Remotely Sensed SST and Chlorophyll-A Concentration (2004–2012)." *Fisheries Research* 173: 122–127. doi:10.1016/j.fishres.2015.10.006.

Rodhouse, P. G., C. D. Elvidge, and P. N. Trathan. 2001. "Remote Sensing of the Global Light-Fishing Fleet: An Analysis of Interactions with Oceanography, Other Fisheries and Predators." *Advances in Marine Biology* 39 (01): 261–278.

Sheldon, M. R., M. J. Fillyaw, and W. Douglas Thompson. 2010. "The Use and Interpretation of The Friedman Test in The Analysis of Ordinal-scale Data in Repeated Measures Designs." *Physiotherapy Research International* 1 (4): 221–228.

Silva, C., I. Andrade, E. Yáñez, S. Hormazabal, M. Á. Barbieri, A. Aranis, and B. Gabriela. 2016. "Predicting Habitat Suitability and Geographic Distribution of Anchovy (Engraulis Ringens) Due to Climate Change in the Coastal Areas off Chile." *Progress in Oceanography* 146: 159–174. doi:10.1016/j.pocean.2016.06.006.

Silverman, B. W. 1986. *Density Estimation for Statistics and Data Analysis*. London: Chapman and Hall.

Solanki, H. U., D. Bhatpuria, and P. Chauhan. 2015. "Signature Analysis of Satellite Derived SSHa, SST and Chlorophyll Concentration and Their Linkage with Marine Fishery Resources." *Journal of Marine Systems* 150 (3): 12–21. doi:10.1016/j.jmarsys.2015.05.004.

Straka, W. C., C. J. Seaman, K. Baugh, K. Cole, E. Stevens, and S. D. Miller. 2015. "Utilization of the Suomi National Polar-orbiting Partnership (NPP) Visible Infrared Imaging Radiometer Suite (VIIRS) Day/night Band for Arctic Ship Tracking and Fisheries Management." *Remote Sensing* 7 (1): 971–989.

Van, H. R., A. B. Griffioen, and O. A. van Keeken. 2017. "Changes in Fish Communities on a Small Spatial Scale, an Effect of Increased Habitat Complexity by an Offshore Wind Farm." *Marine Environmental Research* 126: 26. doi:10.1016/j.marenvres.2017.01.009.

Vinagre, C., V. Fonseca, H. Cabral, and M. J. Costa. 2006. "Habitat Suitability Index Models for the Juvenile Soles, Solea Solea and Solea Senegalensis, in the Tagus Estuary: Defining Variables for Species Management." *Fisheries Research* 82 (1–3): 140–149. doi:10.1016/j.fishres.2006.07.011.

Vu, C. T., T. D. Phan, and D. M. Chandler. 2012. "S3: A Spectral and Spatial Measure of Local Perceived Sharpness in Natural Images." *IEEE Transactions on Image Processing A Publication of the IEEE Signal Processing Society* 21 (3): 934–945. doi:10.1109/TIP.2011.2169974.

Waluda, C. M., C. Yamashiro, C. D. Elvidge, V. R. Hobson, and P. G. Rodhouse. 2004. "Quantifying Light-Fishing for Dosidicus Gigas in the Eastern Pacific Using Satellite Remote Sensing." *Remote Sensing of Environment* 91 (2): 129–133. doi:10.1016/j.rse.2004.02.006.

Waluda, C. M., H. J. Griffiths, and P. G. Rodhouse. 2008. "Remotely Sensed Spatial Dynamics of the Illex Argentinus Fishery, Southwest Atlantic." *Fisheries Research* 91 (2): 196–202. doi:10.1016/j.fishres.2007.11.027.

Wang, W., C. Zhou, Q. Shao, and D. J. Mulla. 2010. "Remote Sensing of Sea Surface Temperature and Chlorophyll-A: Implications for Squid Fisheries in the North-West Pacific Ocean." *International Journal of Remote Sensing* 31 (17–18): 4515–4530. doi:10.1080/01431161.2010.485139.

Wang, Y., J. Zheng, and Y. Cungen. 2014. "Stock Assessment of Chub Mackerel (Scomber Japonicus) in the Central East China Sea Based on Length Data." *Journal of the Marine Biological Association of the United Kingdom* 94 (1): 211–217. doi:10.1017/S0025315413001434.

Yasuda, T., S. Ohshimo, and R. Yukami. 2014. "Fishing Ground Hotspots Reveal Long-Term Variation in Chub Mackerel Scomber Japonicus Habitat in the East China Sea." *Marine Ecology Progress* 501 (501): 239–250. doi:10.3354/meps10679.

Yen, K.-W., L. Hsueh-Jung, Y. Chang, and M.-A. Lee. 2012. "Using Remote-Sensing Data to Detect Habitat Suitability for Yellowfin Tuna in the Western and Central Pacific Ocean." *International Journal of Remote Sensing* 33 (23): 7507–7522. doi:10.1080/01431161.2012.685973.

Yu, W., X. Chen, Y. Qian, Y. Chen, Y. Wei, X. Chen, Y. Qian, and Y. Chen. 2016. "Spatio-Temporal Distributions and Habitat Hotspots of the Winter–Spring Cohort of Neon Flying Squid Ommastrephes Bartramii in Relation to Oceanographic Conditions in the Northwest Pacific Ocean." *Fisheries Research* 175: 103–115. doi:10.1016/j.fishres.2015.11.026.

Zheng, J. 2008. "The Research of Management by Light-Seine in the East China Sea." *Journal of Zhejiang Ocean University* 27(1): 51–59.